IEEE ComSoc IEEE Communications Society
IEEE Open Journal of the Communications Society

Received 18 November 2024; revised 17 December 2024; accepted 19 December 2024. Date of publication 23 December 2024; date of current version 18 April 2025.

Digital Object Identifier 10.1109/OJCOMS.2024.3521293

PANTHER: A Power-Optimized and Accurate Positioning, Navigation, and Timing With High Efficiency and Reliability

MD SADMAN SIRAJ [1] (Graduate Student Member, IEEE), JOSHUA R. ATENCIO [2] (Graduate Student Member, IEEE), AND EIRINI ELENI TSIROPOULOU [1] (Senior Member, IEEE)

(Selected Best Papers of IEEE International Conference on Communications (ICC'24))

[1] School of Electrical, Computer and Energy Engineering, Arizona State University, Tempe, AZ 85281, USA
[2] Department of Electrical and Computer Engineering, University of New Mexico, Albuquerque, NM 87131, USA

CORRESPONDING AUTHOR: E. E. TSIROPOULOU (e-mail: eirini@asu.edu)

The work of Eirini Eleni Tsiropoulou was supported in part by NSF under Award 2219617 and Award 2319994.

ABSTRACT Positioning, Navigation, and Timing (PNT) systems are vital in both military and civilian domains to provide essential support for navigation, situational awareness, and coordinated operations. However, in GPS-denied environments, such as contested military zones or disaster areas, existing PNT solutions face significant limitations, such as signal interference and jamming. To address these challenges, we propose the PANTHER framework, which combines matching theory, coalition game models, and power optimization techniques to deliver a ground-based PNT solution tailored for dynamic and complex operational scenarios. The PANTHER framework introduces a novel ground-based solution designed to support search-and-rescue missions and military operations by using ad-hoc developed anchor nodes to assist the targets' positioning when GPS signals are unavailable. Initially, we develop the Approximate PANTHER (A-PANTHER) framework, utilizing matching theory to enable the anchor node selection for targets located at a Forward Operating Base (FOB). For operations extending beyond the FOB, we present the Accurate PANTHER (Acc-PANTHER) framework, which leverages the coalition game theory to facilitate collaborative selection of anchor nodes by targets, with proven convergence of Nash-individually stable coalitions. Additionally, we optimize the anchor nodes' transmission power using a non-cooperative game-theoretic approach, maximizing their utility with respect to the PNT services, while improving positioning errors for the targets. The existence and uniqueness of a Pure Nash Equilibrium for power levels are demonstrated. Through extensive simulations, the PANTHER framework demonstrates scalability and effectiveness across various military formations, such as line, echelon, column, and wedge, providing a practical and reliable PNT solution for mission-critical scenarios.

INDEX TERMS Positioning, navigation, and timing, power control, matching theory, coalitional game theory, public safety.

I. INTRODUCTION

WITH the rapid evolution of technology, warfare is increasingly shifting towards an era characterized by information dominance and intelligent systems [1]. In this context of future warfare, where information dominance is key, the ability to accurately assess and comprehend the battlefield environment becomes important in order to ensure security and safety. To protect military assets and personnel, precise Positioning, Navigation, and Timing (PNT) systems are essential. The Global Navigation Satellite System (GNSS), particularly the Global Positioning System (GPS), currently serves as the primary PNT solution. However, GPS faces vulnerabilities such as signal interference and jamming, which can result in unreliable or compromised

services [2]. Therefore, developing alternative ground-based PNT solutions is critical [3].

This paper presents a novel ground-based PNT system, named PANTHER. This system integrates matching theory, coalition game models, and power optimization techniques to enhance the secure navigation support during rescue missions and military operations, particularly in environments where GPS is unavailable. PANTHER is designed for practical operational scenarios, incorporating anchor nodes and targets in GPS-denied settings. The PANTHER system has two primary components: the Approximate PANTHER framework, which uses the principles of matching game theory to determine the anchor nodes for each target located at a Forward Operating Base (FOB), i.e., a temporary military encampment in or near an operational area, and the Accurate PANTHER framework, which applies coalition game theory to facilitate the collaborative anchor node selection during rescue missions. Additionally, aiming at improving the operational efficiency of the PANTHER framework, a power optimization model is incorporated to set the transmission power levels of the anchor nodes in order to ensure both high efficiency and reliability in delivering PNT services.

A. RELATED WORK

The challenge of creating precise *alternative PNT solutions* has gained significant attention from numerous nations, driven by the need to enhance both civilian and military functionalities. These solutions are critical for various sectors, such as transportation [4], energy management, emergency response, and military surveillance [5], among others. A framework for enhancing multirobot autonomy through semantic maps is proposed in [6] enabling complex collaborative missions in outdoor environments, particularly in GPS-denied settings. The authors in [7] demonstrate the feasibility of integrating joint localization and imaging functions in future mobile systems using radio reference signals in order to enhance the accuracy and target distinction for economic surveillance solutions at airports. An extrinsic information-aided fingerprint localization algorithm is introduced in [8] targeting at enhancing the vehicle localization accuracy. An improved particle swarm optimization method for Unmanned Aerial Vehicles (UAVs) localization is presented in [9] that reduces the complexity and localization error in GPS-denied environments. Similarly, a UAV localization method is analyzed in [10] that effectively matches oblique UAV images with ortho-photograph satellite imagery to enhance the robustness and precision under varying conditions. A terrain-aided simultaneous localization and mapping (SLAM) algorithm that enables accurate real-time optical navigation of planetary UAVs in GPS-denied environments is designed in [11].

Furthermore, the authors in [12] quantitatively analyze the impact of system time delay on localization accuracy in a multi-antenna very high frequency radiation observation system and introduce a correction method that significantly reduces localization errors caused by this delay. A minimum Quality of Experience maximization scheme for location-dependent augmented reality services in metaverse systems is designed in [13] to address the localization errors and resource management challenges in order to enhance the user fairness and performance. An asynchronous localization method for Integrated Sensing and Communication (ISAC) networks is analyzed in [14] to address the challenges of propagation delay and node mobility towards enhancing the autonomous underwater vehicles' localization accuracy.

Recent alternative PNT solutions have explored *physical layer processing approaches* for localization purposes. An adaptive square-root cubature Kalman filter-based low-cost positioning system is proposed in [37] that combines IMU, ultra-wideband (UWB), and an adaptive noise model to achieve high-precision autonomous inspection in GPS-denied environments. A similar method is presented in [38] by jointly exploiting IMU, stereo camera, GPS, and LiDAR data to enhance accuracy and robustness in both GPS-denied and GPS-enabled environments. The IMU and UWB data are also used in [39] based on a finite-time adaptive relative localization scheme for multi-robot systems in GPS-denied environments. Also, a high-precision indoor localization scheme for autonomous drones is discussed in [40] that uses ultrasonic acoustic signals and a three-stage process to achieve centimeter-level accuracy in GPS-denied environments.

Recent advances in *artificial intelligence and next-generation networking technologies* have introduced sophisticated tools that significantly improve the design and implementation of terrestrial PNT solutions. A convolutional neural network for accurately estimating the users' position and orientation in mobile scenarios using received signal strength (RSS) data is designed in [20]. A two-stage low-complexity method for joint 3D localization and synchronization is described in [21] using multiple RISs. A robust localization scheme for unmanned ground vehicles in GPS-denied environments is analyzed in [22] utilizing multisensor fusion with 3D lidar and inertial measurement unit (IMU) data to enhance positional accuracy under a point-cloud map. A sparse motion removal model is proposed in [23] to enhance the visual localization accuracy in dynamic environments by effectively detecting and eliminating dynamic regions from input frames.

Data analytics techniques have also contributed to the design of alternative PNT solutions. A fusion model is designed in [24] leveraging odometer and ranging measurements for anchor-free localization in multi-target systems. A probabilistic method for passive pedestrian detection and localization in visible light communication systems is proposed in [25] by leveraging blockage status of line-of-sight links and achieving high accuracy in estimating pedestrian size and position. The authors in [26] introduce a two-stage channel estimation model for mm-wave communications that enables centimeter-level localization accuracy using compressed sensing and few-bit analog to digital converters. A cross-view geo-localization method is proposed in [27] by utilizing contrastive attributes mining and

position-aware partitioning. A dual-layer planning approach with pose SLAM is proposed in [28] for autonomous robot exploration in GPS-denied environments, combining local and global planners to enhance exploration efficiency and localization accuracy. A clustering-based cooperative relative localization scheme for UAV swarms is designed in [29] utilizing a coalition formation game model to enhance localization accuracy and efficiency in satellite-denied environments. A voxel-based localization and mapping system is developed in [30] for multi-robot operations in GPS-denied environments, significantly enhancing computational efficiency and reducing communication bandwidth.

B. CONTRIBUTIONS AND OUTLINE

Despite the advancements in alternative PNT solutions, there remains a significant gap in integrating robust theoretical frameworks with practical applications in GPS-denied environments, particularly during rescue missions and military operations. Many existing approaches primarily focus on individual localization techniques without addressing the collaborative identification of anchor nodes and their utilization based on real-time operational needs. Additionally, while some studies emphasize the use of advanced technologies such as artificial intelligence and 6G communication technologies, there is limited research on their combined application in enhancing the targets' positioning and power optimization for ground-based PNT systems. Our proposed PANTHER system aims to fill these gaps by jointly leveraging the matching theory, coalition game models, and power optimization techniques to provide a comprehensive solution tailored for dynamic and challenging operational scenarios. The key contributions of this research work are summarized as follows.

1) A novel PNT solution for GPS-denied environments, named PANTHER, is introduced by developing a ground-based system for search-and-rescue and military operations, using anchor nodes to support the targets' positioning in GPS-denied settings.
2) Initially, the Approximate PANTHER (A-PANTHER) framework is introduced based on the matching theory, for targets residing at a Forward Operating Base (FOB) to select anchor nodes for precise and reliable PNT services.
3) For extended operations outside the FOB, the Accurate PANTHER (Acc-PANTHER) framework is developed based on the coalition game theory to enable the collaborative selection of anchor nodes by the targets. The existence of Nash-individually stable coalitions and their convergence are proven.
4) Then, the transmission power of the anchor nodes is optimized using a non-cooperative game-theoretic model, maximizing the anchor nodes' utility while mitigating the targets' positioning errors. The existence and uniqueness of a Pure Nash Equilibrium for the anchor nodes' power levels are demonstrated.
5) Performance analysis through simulations and real-world testing validates the scalability and effectiveness of the PANTHER solution across various target formations (line, echelon, column, wedge) as derived by the Ranger Handbook [31], and provides insights for practical application in mission-critical scenarios.

TABLE 1. Summary of key notations.

Notation	Description
$\mathcal{S}, \mathcal{N}$	Set of anchor nodes, and targets, respectively
S, N	Total number of anchor nodes, and targets, respectively
$\mathbf{X}_s$	Location and timing of anchor node s
$\hat{\mathbf{X}}_n$	Location and timing of target n
B [bits]	Size of beacon signal
W [Hz]	Bandwidth
P_s [W]	Transmission power of anchor node s
$\mathbf{P}_{-s}$ [W]	Transmission power of all other anchor nodes except s
$P_s^{\max}$ [W]	Maximum transmission power of anchor node s
$d_{s,n}$ [m]	Distance between anchor node s and target n
$G_{s,n}$	Channel gain between anchor node s and target n
$t_{s,n}$ [s]	Total delay for target n to receive each beacon signal from anchor node s
c [$\frac{m}{s}$]	Speed of light
N_0 [$\frac{dBm}{Hz}$]	Power spectral density of ambient noise
I_0 [W]	Ambient noise level
$\boldsymbol{\sigma}_n$	Constellation of anchor nodes chosen by target n
$\boldsymbol{\sigma}_{-n}$	Constellation of anchor nodes chosen by all other targets except n
$\mathcal{K}$	Set of constellations
K	Total number of constellations
$\sum_{\boldsymbol{\sigma}_n} d_{s,n}$ [m]	Sum of distances from the target n to each anchor node in $\boldsymbol{\sigma}_n$
$\sum_{\boldsymbol{\sigma}_n} G_{s,n}$	Sum of channel gains between the target n and each anchor node in $\boldsymbol{\sigma}_n$
$\sum_{\boldsymbol{\sigma}_n} t_{s,n}$ [s]	Sum of total delays between the target n and each anchor node in $\boldsymbol{\sigma}_n$
$\hat{U}_n, U_n$	Approximate and accurate utilities of target n respectively
$\hat{U}_s, U_s$	Approximate and accurate utilities of anchor node s
w_1, w_2	Weights of the denominator of Eq. 2
λ	Balancing parameter for precise PNT service and associated power expenditure
$\mathcal{N}_s$	Group of targets handled by anchor node s
$N_{\max}$	Maximum capacity of targets served by each constellation
f_c [Hz]	Carrier frequency of the beacon signal
$M(n)$	Constellation $k \in \mathcal{K}$ that is related to target $n \in \mathcal{N}$
$M(k)$	Set of targets assigned to the constellation $k \in \mathcal{K}$
$<_n$	Preference relation for each specific target n
$<_k$	Preference relation for each specific constellation k
$\mathcal{C}$	Set of coalitions
$\mathcal{N}_c$	Group of targets in coalition c
$\mathcal{U}(c)$	Utility of coalition c
$\mathcal{P}_s$	Strategy set of anchor node s
$\mathbf{P}^*$	Strategy vector of transmission powers of anchor nodes
G	Non-cooperative game among the anchor nodes
I_1, ITE	Number of iterations for the Acc-PANTHER algorithm and the power control algorithm to converge, respectively
η	Efficiency factor

The remainder of the paper is organized as follows. The ground-based PNT system model is presented in Section II. The A-PANTHER and Acc-PANTHER frameworks are presented in Sections III and IV, respectively. The anchor nodes' power optimization model is analyzed in Section V, while detailed experiments are presented in Section VI. Section VII concludes the paper.

II. GROUND-BASED PNT SYSTEM MODEL

We analyze a practical operational scenario following the principles provided in the Ranger Handbook [31]. This scenario includes a group of dynamically established anchor nodes, denoted as $\mathcal{S} = \{1, \ldots, s, \ldots, S\}$, and a set of

targets, represented by $\mathcal{N} = \{1, \ldots, n, \ldots, N\}$. The locations and timing of the anchor nodes are indicated by $\mathbf{X}_s = (x_s, y_s, z_s, \Delta t_s)$, while the corresponding variables for the targets are expressed as $\hat{\mathbf{X}}_n = (\hat{x}_n, \hat{y}_n, \hat{z}_n, \hat{\Delta} t_n)$. The positions and timings of the anchor nodes (i.e., anchor nodes) are assumed to be known. Each target must decode the signals from four specific beacon transmissions, each of which corresponds to one of four unknowns, i.e., $(\hat{x}_n, \hat{y}_n, \hat{z}_n, \hat{\Delta} t_n)$. The four beacon signals are transmitted from a set of four anchor nodes. This decoding enables the target to determine its own position and time using the multilateration technique [32]. The beacon signals have a size of B [bits], are sent with a constant transmission power P_s [Watts], and utilize an industrial, scientific, and medical (ISM) band with a bandwidth of W Hz. The total delay for the target to receive each beacon signal, including both the transmission and propagation delays, is calculated as:

$$t_{s,n} = \frac{B}{W \cdot \log_2\left[1 + \frac{P_s \cdot G_{s,n}}{\sum_{s' \neq s} P_{s'} \cdot G_{s',n} + I_0}\right]} + \frac{d_{s,n}}{c} \tag{1}$$

with $d_{s,n}$ [m] representing the distance between anchor node s and the target n, and $G_{s,n}$ denoting the corresponding channel gain. Also, c $[\frac{m}{s}]$ stands for the speed of light, and $I_0 = W \cdot N_0$ [W] with $N_0 = -175$ $[\frac{dBm}{Hz}]$, refers to the ambient noise level. Eq. (1) models the complete delay for each beacon signal by combining the effects of both the channel capacity, which is limited by the signal-to-interference-plus-noise ratio (SINR), i.e., first term of Eq. (1), and the physical propagation delay, i.e., second term of Eq. (1). This delay directly impacts the accuracy and reliability of the multilateration technique that is used to determine the target's position, as it affects the time that the target needs in order to decode each signal. Also, the interference modeling inherently includes the contributions of signals from all transmitting anchor nodes $\sum_{s' \neq s} P_{s'}$, regardless of their constellation membership relative to the target device. Specifically, SINR captures interference from all simultaneously transmitting anchors in the system, reflecting the cumulative effect of intra-constellation and inter-constellation interference.

In this system, we utilize CDMA (Code Division Multiple Access) as a practical and cost-effective solution that is compatible with existing low-cost hardware that is suitable to be used in military operations and allows for efficient deployment without requiring specialized frequency allocation for each anchor node. CDMA enables each anchor to transmit simultaneously in the same ISM band while using distinct codes, which makes it possible for the target to differentiate among the signals transmitted from different anchors. Furthermore, the beacon signals serve a dual role in our system. In addition to being used in order for the anchor nodes to estimate the communication links' channel gain conditions, these signals also function as pilot signals for localization purposes, as we further elaborate in the rest of the paper. By decoding these beacon signals, the target can estimate the channel gains for each anchor node, which enhances the accuracy of its position determination. This dual-use approach optimizes the system by leveraging the same set of signals to both estimate the communication and provide the necessary information for precise localization, thus, avoiding additional signaling overhead.

Regarding the interaction and interference among the codes, Eq. (1) incorporates the SINR in the calculation of total delay, capturing the impact of both inter-anchor interference and ambient noise. The SINR-based channel capacity reflects how interference among anchor signals is managed, leveraging the orthogonality of the codes to maintain a high signal-to-noise ratio. We also recognize the importance of geometric factors, such as the spatial distribution of anchors and devices. These factors are directly addressed in our target constellation selection mechanism. The proposed system ensures that each target chooses a set of four anchor nodes from its vicinity, and prioritizes strong channel conditions and minimal latency. This approach inherently considers the geometric arrangement of anchors relative to the target, as well as the associated channel gains, which are estimated through the decoding of the beacon signals.

The objective of each target is to choose a constellation $\boldsymbol{\sigma}_n = \{s_i, s_j, s_k, s_m\}$, where $i \neq j \neq k \neq m$ and all elements s_i, s_j, s_k, s_m belong to the set $\mathcal{S}$. This constellation must be located near the target, provide strong channel conditions for the receiving signals, and minimize the total latency. Thus, the utility for the target, in relation to obtaining PNT services from its chosen constellation $\boldsymbol{\sigma}_n$, is expressed as follows:

$$U_n(\boldsymbol{\sigma}_n, \boldsymbol{\sigma}_{-n}) = \frac{\frac{\sum_{\sigma_n} G_{s,n}}{\max\left\{\sum_{\sigma_n} G_{s,n}\right\}_{\forall n \in \mathcal{N}}}}{w_1 \frac{\sum_{\sigma_n} t_{s,n}}{\max\left\{\sum_{\sigma_n} t_{s,n}\right\}_{\forall n \in \mathcal{N}}} + w_2 \frac{\sum_{\sigma_n} d_{s,n}}{\max\left\{\sum_{\sigma_n} d_{s,n}\right\}_{\forall n \in \mathcal{N}}}} \tag{2}$$

with $w_1 + w_2 = 1, w_1, w_2 > 0$, and the set of potential constellations for the remainder of the analysis is represented by $\mathcal{K} = \{1, \ldots, k, \ldots, K\}$, where, $K = \frac{S!}{4!(S-4)!}$. The physical meaning of Eq. (2) captures the core requirements for effective PNT by balancing the following factors: (i) channel quality: The term $\sum_{\boldsymbol{\sigma_n}} G_{s,n}$ represents the aggregate channel gain from the selected constellation and quantifies the overall quality of the signals received from the anchor nodes. Thus, maximizing this sum ensures that the target has a strong and stable connection to the selected anchor nodes, which is essential for accurate signal decoding and position estimation; (ii) latency: The term $\sum_{\boldsymbol{\sigma}_n} t_{s,n}$ denotes the total delay, i.e., transmission and propagation latency from each anchor node in the chosen constellation. Thus, lower latency contributes to timely and responsive PNT services, particularly in dynamic or time-sensitive environments which are critical for military applications; and (iii) spatial proximity: The term $\sum_{\boldsymbol{\sigma}_n} d_{s,n}$ represents the sum of distances from the target to each anchor node in $\boldsymbol{\sigma}_n$, and it is beneficial for the target's PNT services to choose nearby

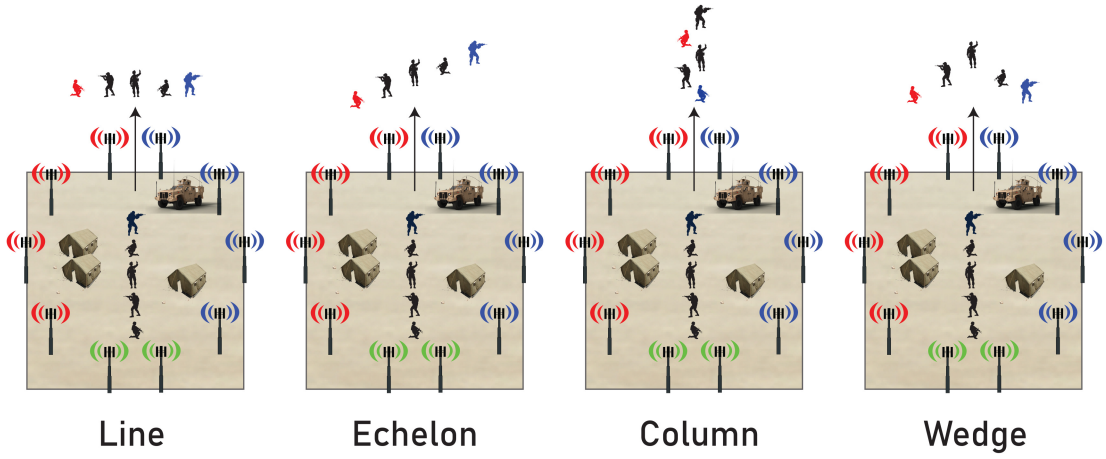

FIGURE 1. File formation within the FOB and Line, Echelon, Column, and Wedge formations during reconnaissance – soldier colors represent preferences for the anchor nodes based on proximity, and black-colored soldiers act as placeholders, illustrating how formation geometry affects the anchor selection.

anchor nodes in order to minimize the effects of path loss and potential interference, which improves signal reliability and reduces the likelihood of errors in the localization process.

The primary goal is to enhance the PNT services provided by the anchor nodes to their designated targets. Each constellation is structured to optimize the benefit delivered to the targets, primarily by ensuring high transmission power, which guarantees a strong received signal and, therefore, accurate positioning and timing services. However, the power efficiency is also critical, especially since the anchor nodes often rely on limited, self-sustaining power sources (such as batteries or solar cells). In this setup, the anchor nodes operate in a power-saving mode unless chosen by a target. This approach conserves the anchor nodes' energy by prioritizing active, high-power transmission only for selected constellations. Thus, the utility of an anchor node in offering PNT services to its associated targets can be described as follows:

$$U_s(\boldsymbol{\sigma}, P_s, \mathbf{P}_{-s}) = \sum_{\forall n \in \mathcal{N}_s} U_n(\boldsymbol{\sigma}_n, \boldsymbol{\sigma}_{-n}) - \lambda P_s \tag{3}$$

where $\lambda > 0$ represents the balance between the advantage of transmitting at higher power for precise PNT services and the associated power expenditure, where $\mathcal{N}_s$ captures the group of targets being handled by anchor node s.

III. APPROXIMATE PANTHER BASED ON MATCHING GAMES

In realistic search-and-rescue and military operations, before launching the rescue or patrol missions, the targets are tactically arranged in a file formation near the Forward Operating Base (FOB) and positioned close to the anchor nodes (Fig. 1). Each target seeks to optimize its utility (Eq. (2)) by intelligently selecting a constellation $\boldsymbol{\sigma}_n$, aiming to enhance its received PNT services. However, each constellation has a maximum capacity of serving $N_{\max}$ targets to prevent overloading and maintain the quality of PNT services. Although the anchor nodes could, in theory, broadcast signals (e.g., using spread-spectrum techniques) to all the targets, the capacity limitations are implemented to manage the power resources efficiently and avoid excessive load on communication channels, which can degrade the signal's quality in high-density deployments. It is noted that spread-spectrum techniques allow for broadcasting to multiple targets, however, excessive load degrades the SINR and reduces the effectiveness of the spread spectrum, especially in interference-heavy environments, such as the ones examined in the PANTHER framework. Thus, the targets extend pairing invitations to the anchor nodes, while the latter ones accept them or not under the criterion of maximizing their achieved utility. This scenario can be appropriately modeled using the principles of matching theory, by designing a many-to-one matching framework.

Definition 1 (Matching Game): Consider two disjoint sets: a set of targets $\mathcal{N}$ and a set of constellations $\mathcal{K}$, and $M(n)$ representing the constellation $k \in \mathcal{K}$ that is related to target $n \in \mathcal{N}$ and $M(k)$ capturing the set of targets assigned to the constellation $k \in \mathcal{K}$. A match M is defined as a mapping from $\mathcal{N}$ to $\mathcal{K}$, satisfying the following constraints: $(\mathbf{C}_1)$: $|M(n)| \leq 1, \forall n \in \mathcal{N}$; $(\mathbf{C}_2)$: $|M(k)| \leq N_{\max}, \forall k \in \mathcal{K}$; $(\mathbf{C}_3)$: $M(n) \in \mathcal{K}$ if and only if $M(k) \in \mathcal{N}$; and $(\mathbf{C}_4)$: $n \in M(k) \Leftrightarrow M(n) = k$. The size of the match $M(\cdot)$ is denoted as $|M(\cdot)|$. If $M(n) = \emptyset$, the target n has no constellation, and similarly, if $M(k) = \emptyset$, then no target is assigned to constellation k.

For each target n, the preferred constellation is the one that maximizes its utility (Eq. (2)). The utility of target n depends not only on its chosen constellation $\boldsymbol{\sigma}_n$ but also on the constellation selections of other targets $\boldsymbol{\sigma}_{-n}$, through the factor $\mathbf{P}_{-s}(\boldsymbol{\sigma}_{-n})$ due to the interference stemming from the transmissions of the other anchor nodes. It is noted that $\mathbf{P}_{-s}(\boldsymbol{\sigma}_{-n})$ denotes the transmission power of all the anchor nodes that do not belong in the constellation chosen by target n. This dependence stems from the transmission power settings of all the anchor nodes, which are influenced by the collective constellation choices of the targets. This

phenomenon, known as externality in matching theory, plays a key role in the decision-making process of the targets in terms of selecting anchor nodes. In the initial phase of the matching process, when the targets are within the FOB, we employ the Approximate PANTHER algorithm to pair the targets with constellations, assuming no externalities are present during this matching phase, i.e., the interference stemming from the other anchor nodes is neglected for the initial matching process (as captured in the $t_{s,n}$ factor of Eq. (4)). Thus, the target's utility can be reformulated as follows.

$$\hat{U}_n(\boldsymbol{\sigma}_n) = \frac{\frac{\sum_{\boldsymbol{\sigma}_n} G_{s,n}}{\max\left\{\sum_{\boldsymbol{\sigma}_n} G_{s,n}\right\}_{\forall n\in\mathcal{N}}}}{w_1 \frac{\left(\sum_{\boldsymbol{\sigma}_n} \frac{B}{W\cdot\log_2\left(1+\frac{P_s G_{s,n}}{I_0}\right)} + \frac{d_{s,n}}{c}\right)}{\max\left\{\sum_{\boldsymbol{\sigma}_n} t_{s,n}\right\}_{\forall n\in\mathcal{N}}} + w_2 \frac{\sum_{\boldsymbol{\sigma}_n} d_{s,n}}{\max\left\{\sum_{\boldsymbol{\sigma}_n} d_{s,n}\right\}_{\forall n\in\mathcal{N}}}} \tag{4}$$

Thus, the utility function of the anchor nodes can be reformulated as follows: $\hat{U}_s(\boldsymbol{\sigma}, P_s) = \sum_{\forall n\in\mathcal{N}_s} \hat{U}_n(\boldsymbol{\sigma}_n) - \lambda P_s$.

Definition 2 (Preference Relation): A preference relation represented as $\prec$ denotes a binary relationship involving elements from sets $\mathcal{N}$ and $\mathcal{K}$. This relation is both exhaustive and transitive, thus, establishing a hierarchy of preferences among these elements. The preference relation $\prec_n$ for each specific target n can be expressed as follows:

$$k \succ_n k' \Leftrightarrow \hat{U}_n(k) > \hat{U}_n\left(k'\right) \tag{5}$$

Additionally, the preference relation $\prec_k$ for each specific constellation k is evaluated through the following criteria:

$$n \succ_k n' \Leftrightarrow \sum_{k} \sum_{\forall n''\in\mathcal{N}_s\cup\{n\}} \hat{U}_{n''}(k) - \lambda P_s > \sum_{k} \sum_{\forall n''\in\mathcal{N}_s\cup\{n'\}} \hat{U}_{n''}(k) - \lambda P_s \tag{6}$$

where $k = s_i, s_j, s_k, s_m$.

Based on the criteria specified in Definition 2, the preference rankings for both constellations and targets are established. These rankings are then utilized to form mutually beneficial pairings between the constellations and the targets. The process of matching is encapsulated in the Approximate PANTHER (A-PANTHER) Algorithm 1.

The core concepts of the A-PANTHER algorithm are described as follows. Initially, all the targets remain unpaired and are free to connect with any constellation that is available. Unmatched targets generate pairing invitations directed towards their preferred constellations. If a constellation can accommodate the targets, it will continuously select its preferred targets for pairing from those who have expressed interest. If a target extends a pairing invitation to a constellation that does not accept it, this prompts the constellation to seek a more preferable target, resulting in the rejection of the initial target. Thus, the targets will avoid sending additional invitations to constellations that show no interest in order to optimize their time management. The A-PANTHER algorithm concludes when either all the constellations are at full capacity or every target has already been successfully paired.

Algorithm 1 Approximate PANTHER (A-PANTHER) Algorithm

Input: $\mathcal{K}, \mathcal{N}, \mathcal{S}, \{G_{s,n}\}_{\substack{\forall s\in\mathcal{S}\\ \forall n\in\mathcal{N}}}, \{t_{s,n}\}_{\substack{\forall s\in\mathcal{S}\\ \forall n\in\mathcal{N}}}, \{d_{s,n}\}_{\substack{\forall s\in\mathcal{S}\\ \forall n\in\mathcal{N}}}, \{P_s\}_{\forall s\in\mathcal{S}}, B, W, I_0, c, \lambda$
Output: M
Initialization: $\mathcal{N}^* \leftarrow \mathcal{N}$, $\mathcal{K}_n \leftarrow \{k | \forall s \in \mathcal{S}, \forall k \in \mathcal{K}\}, \forall n \in \mathcal{N}$
while $\mathcal{N}^* \neq \emptyset$ and $\mathcal{K}_n \neq \emptyset, \exists n \in \mathcal{N}^*$ **do**
  for $n \in \mathcal{N}^*$ **do**
    Target n chooses its preferred constellation from the available ones and initiates a pairing request by sending a pair invitation (based on Eq. (5)).
  end for
  for $k \in \mathcal{K}$ **do**
    if $(|M(k)| < N_{\max}) \wedge (k$ received pair invitation$)$ **then**
      Constellation k chooses its preferred targets for pairing from the pool of targets that have extended partnership invitations (based on Eq. (6)).
      Eliminate constellation k from the alternate options considered by targets that extended invitations but did not receive acceptance.
    end if
  end for
end while

IV. ACCURATE PANTHER BASED ON COALITION GAMES

Given the stable matching pair through the A-PANTHER framework, the targets can effectively utilize the PNT services while remaining within the FOB. However, when the targets extend their operations beyond the FOB for search-and-rescue missions, they adopt various tactical formations (see Fig. 1). Moreover, as discussed in Section III, the outcomes generated by the A-PANTHER algorithm only approximate stable solutions due to the externalities. Thus, a coalition game framework is developed to enhance the matching results, building on the A-PANTHER algorithm's findings while addressing the complications introduced by externalities and the varied formations of the targets beyond the FOB.

Definition 3 (Coalition Game): A coalition game is formally denoted as $(\mathcal{N}, \mathcal{C}, \mathcal{U})$, where $\mathcal{N}$ represents the set of targets, and $\mathcal{C}$ denotes the set of coalitions. Each coalition c corresponds to a configuration selected by a specific group of targets $\mathcal{N}_c = \{1, \ldots, n, \ldots, N_s\}$. Every target selects a single coalition. The utility for coalition c is given by $\mathcal{U}(c) = \sum_{\forall n\in\mathcal{N}_s} \mathcal{U}_n(c)$.

Definition 4 (Switching Operations): The coalition game includes various forms of switching operations (SO).

Algorithm 2 Accurate PANTHER (Acc-PANTHER) Algorithm

Input: $\mathcal{C}_{\text{initial}}$ from A-PANTHER, same inputs as in A-PANTHER
Output: Coalition Formation $\mathcal{C}^*$
Initialization: Targets move from $\hat{\mathbf{X}}_n^{\text{initial}}$ to $\hat{\mathbf{X}}_n^{\text{final}}$ and calculate U_n (Eq. (2)) using $\mathcal{C}_{\text{initial}}$ from the outcome of the A-PANTHER algorithm.
repeat
  Randomly select a target n and its coalition c
  if n does not belong to any coalition **then**
    $c = \underset{c^* \in \mathcal{C}}{\text{argmax}}\{(\mathcal{U}(c^* \cup \{n\}) - \mathcal{U}(c^*) | \mathcal{U}(c^* \cup \{n\}) - \mathcal{U}(c^*) > 0) \ \wedge (N_{c^*} + 1 \leq N_{\max})\}$
    $\mathcal{C} = \{\mathcal{C} \setminus \{n\}\} \cup \{c \cup \{n\}\}$
  else
    Another coalition $c', c' \neq c$ is randomly selected
    if $N_{c'} + 1 \leq N_{\max}$ **then**
      if $\mathcal{U}(c \setminus \{n\}) + \mathcal{U}(c' \cup \{n\}) > \mathcal{U}(c) + \mathcal{U}(c')$ **then**
        $\mathcal{C} = \{\mathcal{C} \setminus \{c, c'\}\} \cup \{c \setminus \{n\}\} \cup \{c' \cup \{n\}\}$
      end if
    else
      Randomly select a target n' of coalition c'
      if $\mathcal{U}((c \setminus \{n\}) \cup \{n'\}) + \mathcal{U}((c' \setminus \{n'\}) \cup \{n\}) > \mathcal{U}(c) + \mathcal{U}(c')$ **then**
        $\mathcal{C} = \{\mathcal{C} \setminus \{c, c'\}\} \cup \{(c \setminus \{n\}) \cup \{n'\}\} \cup \{(c' \setminus \{n'\}) \cup \{n\}\}$
      end if
    end if
  end if
  Update c to the current coalition of n
  if $\mathcal{U}(c \setminus \{n\}) > \mathcal{U}(c)$ **then**
    $\mathcal{C} = \{\mathcal{C} \setminus \{c\}\} \cup \{c \setminus \{n\}\}$
  end if
until no further updates of the targets

SO 1: A target n not currently in any coalition joins coalition c if $\exists c = arg\,max_{c^* \in \mathcal{C}}\{\mathcal{U}(c^* \cup \{n\}) - \mathcal{U}(c^*) | \mathcal{U}(c^* \cup \{n\}) - \mathcal{U}(c^*) > 0\}$.

SO 2: For $n \in c, n$ leaves from c if $\mathcal{U}(c \setminus \{n\}) > \mathcal{U}(c)$, thus, $\mathcal{C} = \{\mathcal{C} \setminus \{c\}\} \cup \{c \setminus \{n\}\}$.

SO 3: For $n \in \mathcal{N}_c$ and coalition c', n leaves from the original coalition $c \neq c'$ and joins another coalition c' if $\mathcal{U}(c \setminus \{n\}) + \mathcal{U}(c' \cup \{n\}) > \mathcal{U}(c) + \mathcal{U}(c')$, thus, $\mathcal{C} = \{\mathcal{C} \setminus \{c, c'\}\} \cup \{c \setminus \{n\}\} \cup \{c' \cup \{n\}\}$.

SO 4: For $n \in c$ and $n' \in c', n \neq n'$, n and n' switch coalitions if $\mathcal{U}((c \setminus \{n\}) \cup \{n'\}) + \mathcal{U}((c' \setminus \{n'\}) \cup \{n\}) > \mathcal{U}(c) + \mathcal{U}(c')$, thus, $\mathcal{C} = \{\mathcal{C} \setminus \{c, c'\}\} \cup \{(c \setminus \{n\}) \cup \{n'\}\} \cup \{(c' \setminus \{n'\}) \cup \{n\}\}$.

Utilizing the switching operations outlined in Definition 4, we develop the Accurate PANTHER (Acc-PANTHER) algorithm, as demonstrated in Algorithm 2. The Acc-PANTHER algorithm is responsible for forming stable coalitions among targets and constellations and ensuring continuous access to PNT services during their operational activities. In the following analysis, we show that the Acc-PANTHER algorithm converges to a stable matching among the targets and constellations, without experiencing blocking pairs, while the determined matching concludes a Nash-Individually stable coalition formation.

Definition 5 (Blocking Pairs): If $\exists n \in \mathcal{N}$, $\exists k \in \mathcal{K}$ satisfying $M(n) + k$, $k >_n M(n)$, and $n >_n n' \in M(k)$ in matching M, then (n, k) is a blocking pair.

Definition 6 (Stable Match): A match M is a stable match if there are no blocking pairs in the match.

Theorem 1: Acc-PANTHER algorithm will converge to a stable match in a finite number of iterations.

Proof: The target's preference list is finite, allowing each target to send an invitation to each constellation at most once. The constellations can only either accept or reject these invitations. Therefore, the Acc-PANTHER algorithm converges in the worst-case scenario, where all constellations reject the target. Assuming that the final match is not stable, there must exist at least one blocking pair (n, k) such that $M(n) \neq k$, $k >_n M(n)$, and $n >_k n' \in M(k)$. During the matching process, each target sends an invitation to its most preferred constellation based on its preference list. If it is the case that $k >_n M(n)$, the target must have sent the invitation to k prior to being paired. The condition $M(n) \neq k$ implies that k prefers n' $(M(n') = k)$ over n. Therefore, k has no desire to break up the current matching with n' in favor of pairing with n, meaning that $n >_k n' \in M(k)$ does not hold true. As a result, there can be no blocking pair in the final match, which confirms that the final match is stable, and the Acc-PANTHER algorithm converges in a finite number of iterations. ■

Definition 7 (Nash-Individually Stable Coalition Formation): A coalition formation $\mathcal{C}^*$ is a Nash-Individually Stable Coalition if no target of the coalition can increase its utility by switching coalitions.

Theorem 2 (Existence of a Nash-Individually Stable Coalition Formation): The Acc-PANTHER algorithm identifies a Nash-Individually stable coalition formation $\mathcal{C}^*$.

Proof: Assuming initially that the coalition formation $\mathcal{C}$ produced by the Acc-PANTHER algorithm is not Nash-Individually stable. In this scenario, at least one of the following conditions must hold:

1) $\exists n \notin \mathcal{C}, \exists c = \underset{c^* \in \mathcal{C}}{\text{argmax}}\{\mathcal{U}(c^* \cup \{n\}) - \mathcal{U}(c^*) | \mathcal{U}(c^* \cup \{n\}) - \mathcal{U}(c^*) > 0\}$;
2) $\exists n \in c$, satisfying $\mathcal{U}(c \setminus \{n\}) > \mathcal{U}(c)$;
3) $\exists n \in c, \exists c', c \neq c'$, satisfying $\mathcal{U}(c \setminus \{n\}) + \mathcal{U}(c' \cup \{n\}) > \mathcal{U}(c) + \mathcal{U}(c')$; and
4) $\exists n \in c$, $\exists n' \in c'$, and $c \neq c'$, satisfying $\mathcal{U}((c \setminus \{n\}) \cup \{n'\}) + \mathcal{U}((c' \setminus \{n'\}) \cup \{n\}) > \mathcal{U}(c) + \mathcal{U}(c')$.

If any of these conditions are met, the targets will execute the appropriate switching operations as defined in Definition 4. Therefore, the coalition formation cannot be final, as the targets would continue to engage in switching operations, contradicting our initial assumption.

Thus, the Acc-PANTHER algorithm must converge to a Nash-Individually stable coalition formation. ■

Theorem 3 (Convergence): Acc-PANTHER algorithm converges in a finite number of iterations to a Nash-Individually Stable Coalition Formation.

Proof: The coalition game involves a sequence of transitions between different target coalitions, where each transition occurs only if it results in an improved coalition utility. Since each constellation has a limit $N_{\max}$ on the number of targets it can accommodate, and the utility of any coalition is capped at a certain maximum, the total number of possible transitions is bounded. Therefore, the Acc-PANTHER algorithm converges in a finite number of iterations to a Nash-Individually Stable Coalition Formation. ■

To dynamically update the PANTHER system in real time as the users and anchor nodes move, the PANTHER framework can be executed in a periodic manner using periodic execution intervals. In this setup, the framework could operate based on scheduled, time-driven updates where each anchor recalibrates and reassesses target-anchor associations at fixed intervals. This periodic approach reduces the computational load and mitigates the need for complex synchronization protocols by relying on each anchor's updates.

V. ANCHOR NODES' POWER OPTIMIZATION

Based on the Acc-PANTHER algorithm, each target has selected the set of anchor nodes to optimize its PNT service. However, each anchor node also needs to optimize the transmission power of its beacon signals in order to optimize the PNT service offered to the targets. Given that in realistic ground-based PNT systems, the coordination among the anchor nodes may not be feasible and it can introduce additional overhead (both computational and interference-related overhead), we formulate a non-cooperative game among the anchor nodes to determine their transmission power level. The corresponding optimization problem for each anchor node is defined as follows:

$$\max_{P_s} \; U_s(\boldsymbol{\sigma}, P_s, \mathbf{P}_{-s}) \tag{7a}$$

$$\text{s.t.} \quad 0 < P_s \leq P_s^{\max} \tag{7b}$$

where $\boldsymbol{\sigma}$ denotes the selected constellation vector of all the targets, P_s is the transmission power of the anchor node s, $\mathbf{P}_{-s}$ is the transmission power vector of all other anchor nodes, and $P_s^{\max}$ is the maximum transmission power of the anchor node. Please note that in common ground-based PNT solutions, the anchor nodes are mobile ad-hoc developed access points with limited energy availability, thus, their maximum transmission power is constrained. Additionally, these power allocations are important in terms of managing the interference across different targets, as they directly impact the interference levels experienced within the network.

The non-cooperative game is defined as follows: $G = [\mathcal{S}, \{\mathcal{P}_s\}_{\forall s\in\mathcal{S}}, \{U_s\}_{\forall s\in\mathcal{S}}]$, where $\mathcal{S} = \{1, \ldots, s, \ldots, S\}$ is the set of anchor nodes, i.e., anchor nodes, $\mathcal{P}_s = [0, P_s^{max}]$ is the strategy set, and $U_s(\boldsymbol{\sigma}, P_s, \mathbf{P}_{-s})$ is the utility function of the anchor nodes.

Definition 8 (Pure Nash Equilibrium): A strategy vector $\mathbf{P}^* = [P_1^*, \ldots, P_s^*, \ldots, P_S^*]$ is a PNE of the non-cooperative game $G = [\mathcal{S}, \{\mathcal{P}_s\}_{\forall s\in\mathcal{S}}, \{U_s\}_{\forall s\in\mathcal{S}}]$ if for every anchor node s the following condition holds true:

$$U_s\left(P_s^*, \mathbf{P}_{-s}^*\right) \geq U_s\left(P_s, \mathbf{P}{-s^*}\right), \quad \forall P_s \in \mathcal{P}_s$$

Our goal is to determine the transmission power of each anchor node in order to maximize its utility, while achieving the converge to a unique PNE.

Theorem 4 (Existence of PNE): A PNE $\mathbf{P}^* = [P_1^*, \ldots, P_s^*, \ldots, P_S^*]$ exists for the non-cooperative game $G = [\mathcal{S}, \{\mathcal{P}_s\}_{\forall s\in\mathcal{S}}, \{U_s\}_{\forall s\in\mathcal{S}}]$.

Proof: To prove the existence of a PNE, we need to demonstrate that the non-cooperative game G qualifies as a concave n-person game [33]. This requires satisfying two main conditions: (i) the strategy set $\mathcal{P}_s$ must be convex, closed, and bounded; and (ii) the payoff function $U_s(P_s, \mathbf{P}_{-s})$ should be continuous in $\mathbf{P}$ and concave in P_s. The first condition is met, given the structure of the anchor node's strategy set $\mathcal{P}_s$, while continuity in $\mathbf{P}$ is guaranteed by the utility function based on Eq. (3). Next, we proceed to show the concavity of $U_s(P_s, \mathbf{P}_{-s})$ with respect to P_s. For simplicity in the notation, we set: $\alpha = \frac{\sum_{\sigma_n} G_{s,n}}{\max\{\sum_{\sigma_n} G_{s,n}\}}$, $\beta = w_2 \frac{\sum_{\sigma_n} d_{s,n}}{\max\{\sum_{\sigma_n} d_{s,n}\}}$, and $\gamma = w_1 \frac{1}{\max\{\sum_{\sigma_n} t_{s,n}\}}$ and we derive the

$$\frac{\partial U_s}{\partial P_s} = \sum_{\forall n\in N_s} \left(\frac{B}{W} \frac{\ln 2}{\ln^2\left(1 + \frac{P_s G_{s,n}}{\sum_{s'\neq s} P_{s'} G_{s',n} + I_0}\right)} \cdot \frac{G_{s,n}}{\sum_{s'\neq s} P_{s'} G_{s',n} + I_0 + P_s G_{s,n}} \cdot \frac{\alpha\gamma}{\left(\gamma \sum_{\sigma_n} t_{s,n} + \beta\right)^2} \right) - \lambda \tag{8}$$

$$\frac{\partial^2 U_s}{\partial {P_s}^2} = \sum_{\forall n\in N_s} \left(\frac{\partial A}{\partial P_s}\mathcal{B}\Gamma + \frac{\partial \mathcal{B}}{\partial P_s} A\Gamma + AB\frac{\partial \Gamma}{\partial P_s} \right) = \sum_{\forall n\in N_s} A\mathcal{B}^2\Gamma \left(-\frac{2}{\ln\left(1 + \frac{P_s G_{s,n}}{\sum_{s'\neq s} P_{s'} G_{s',n} + I_0}\right)} - 1 + \frac{A}{\left(\gamma \sum_{\sigma_n} t_{s,n} + \beta\right)} \right) < 0 \tag{9}$$

first order derivative in Eq. (8), shown at the bottom of the page.

For simplicity in the notation, we set:

$$A = \frac{\ln 2}{\ln^2\left(1 + \frac{P_s G_{s,n}}{\sum_{s' \neq s} P_{s'} G_{s',n} + I_0}\right)}$$

$$\mathcal{B} = \frac{G_{s,n}}{\sum_{s' \neq s} P_{s'} G_{s',n} + I_0 + P_s G_{s,n}}$$

$$\Gamma = \frac{\alpha\gamma}{\left(\gamma \sum_{\sigma_n} t_{s,n} + \beta\right)^2}$$

and we determine the second-order derivative in Eq. (9), shown at the bottom of the previous page which is negative given that $\frac{B}{W} \frac{1}{\ln(1+\frac{P_s G_{s,n}}{\sum_{s' \neq s} P_{s'} G_{s',n} + I_0})(\gamma \sum_{\sigma_n} t_{s,n} + \beta)(2 + \ln(1 + \frac{P_s G_{s,n}}{\sum_{s' \neq s} P_{s'} G_{s',n} + I_0}))} < 1$. As a result, the utility function $U_s(P_s, \mathbf{P}_{-s})$ is concave with respect to P_s, indicating that the non-cooperative game G is a concave n-person game, and ensures the existence of a PNE. ■

Definition 9 (Diagonal Strict Concavity): Let G be a non-cooperative game with a pseudogradient denoted by $\lambda(\mathbf{P}, \mathbf{r})$:

$$\lambda(\mathbf{P}, \mathbf{r}) = \begin{pmatrix} r_1 \nabla_1 U_1(\mathbf{P}) \\ \vdots \\ r_S \nabla_S U_S(\mathbf{P}) \end{pmatrix}$$

where $\mathbf{P} = [P_1, \ldots, P_s]$ and $\mathbf{r} = [r_1, \ldots, r_s]$. The function $\sigma(\mathbf{P}, \mathbf{r}) = \sum_{s=1}^{S} r_s U_s(\mathbf{P})$, where $\mathbf{r} \geq \mathbf{0}$, is said to be diagonally strictly concave for $\mathbf{P} \in \mathbb{R}$ and a fixed $\mathbf{r} \geq \mathbf{0}$, if for any two points $\mathbf{P}^0, \mathbf{P}^1 \in \mathbb{R}$, the following inequality holds:

$$\left(\mathbf{P}^1 - \mathbf{P}^0\right)' \lambda\left(\mathbf{P}^0, \mathbf{r}\right) + \left(\mathbf{P}^0 - \mathbf{P}^1\right)' \lambda\left(\mathbf{P}^1, \mathbf{r}\right) > 0.$$

Theorem 5: The function representing the weighted sum of the anchor nodes' utilities, given as $\sigma(\mathbf{P}, \mathbf{r}) = \sum_{s=1}^{S} r_s U_s(\mathbf{P})$, exhibits diagonal strict concavity for a particular weight vector $\bar{\mathbf{r}} > \mathbf{0}$.

Proof: Let us denote with $\Lambda(\mathbf{P}, \bar{\mathbf{r}})$ the Jacobian matrix of $\lambda(\mathbf{P}, \bar{\mathbf{r}})$. To prove this theorem, it suffices to show that the symmetric matrix $\Lambda(\mathbf{P}, \bar{\mathbf{r}}) + \Lambda'(\mathbf{P}, \bar{\mathbf{r}})$ is negative definite for all $\mathbf{P} \in \mathbb{R}$, in accordance with [33, Th. 6]. Referring to the Lemma in [34], proving that $\Lambda(\mathbf{P}, \bar{\mathbf{r}}) + \Lambda'(\mathbf{P}, \bar{\mathbf{r}})$ is negative definite requires verifying the following: (C1) $U_s(P_s, \mathbf{P}_{-s})$ is strictly concave in P_s, (C2) $U_s(P_s, \mathbf{P}_{-s})$ is convex in $\mathbf{P}_{-s}$, and (C3) there exists some $\bar{\mathbf{r}} > 0$ such that $\sigma(\mathbf{P}, \bar{\mathbf{r}})$ is concave in $\mathbf{P}$. The first condition, (C1), holds as demonstrated in Theorem 2. To prove (C2), we determine the second-order derivative $\frac{\partial^2 U_s}{\partial P_{s'}{}^2}$ in Eq. (10), shown at the bottom of the next page. Thus, the condition (C2) holds true. Similarly, by appropriately choosing $\mathbf{r} > \mathbf{0}$, we derive that $\sigma(\mathbf{P}, \mathbf{r})$ is concave in $\mathbf{P}$. ■

Theorem 6 (Existence of a Unique PNE): The non-cooperative game G possesses exactly one PNE.

Proof: According to [33, Th. 2], if $\sigma(\mathbf{P}, \bar{\mathbf{r}})$ is a diagonally strictly concave function for some $\bar{\mathbf{r}} > 0$, then the equilibrium point is the unique PNE of the game G. ■

Algorithm 3 Acc-PANTHER Power Control Algorithm

Input: $\mathcal{C}^*$ from Acc-PANTHER, same inputs as in Acc-PANTHER, $\{P_s\}_{\forall s \in \mathcal{S}}$
Output: Unique NE $\mathbf{P}^* = [P_1^*, \ldots, P_s^*, \ldots, P_S^*]$
Initialization: $ite = 0$, $Convergence = 0$, $\mathbf{P}|_{ite=0}$
while $Convergence == 0$ **do**
  $ite = ite + 1$
  $K_s = 0, \forall s \in \mathcal{S}$
  for $s = 1$ to S **do**
    $P_s^*|_{ite} = arg\,max_{P_s} U_s(\boldsymbol{\sigma}, P_s, \mathbf{P}_{-s}|_{ite-1})$
    Calculate $U_s(\boldsymbol{\sigma}, P_s|_{ite}, \mathbf{P}_{-s}|_{ite-1})$ (based on Eq. (3))
    if $(|U_s(\boldsymbol{\sigma}, P_s|_{ite}, \mathbf{P}_{-s}|_{ite-1}) - U_s(\boldsymbol{\sigma}, P_s|_{ite-1}, \mathbf{P}_{-s}|_{ite-2})| \leq \epsilon) \wedge (ite \neq 1)$ **then**
      $K_s = 1$
    end if
  end for
  if $\sum_{\forall s \in \mathcal{S}} K_s == S$ **then**
    $Convergence = 1$
  end if
end while

To find the unique PNE in this non-cooperative game G, a best response dynamics approach can be utilized [35]. Based on this analysis, the transmission power of the anchor nodes is derived to maximize their utility and further contribute to the mitigation of the targets' positioning error.

Theorem 7 (Complexity): The computational complexity of the overall framework in the worst-case scenario is $O((I_1 + \text{ITE}) \cdot N \cdot S)$, where I_1 and ITE are the number of iterations for the Acc-PANTHER algorithm and the power control algorithm to converge, respectively.

Proof: Each target sends invitations to each constellation, thus, the complexity of this operation in the worst case scenario is: $O(N \cdot S \cdot K)$. If the Acc-PANTHER algorithm needs I_1 iterations to converge, then, its complexity is: $O(I_1 \cdot N \cdot S \cdot K)$. If the power control algorithm, following the principles of best response dynamics, needs ITE iterations to converge, then, its complexity is: $O(ITE \cdot N \cdot S)$. Thus, the complexity of the overall framework is $O((I_1 \cdot K + ITE) \cdot N \cdot S)$. ■

The algorithm to determine the transmission powers of the anchor nodes is presented in Algorithm 3.

VI. EVALUATION AND RESULTS

In this section, we introduce a simulation-based assessment to illustrate the operational attributes of the A-PANTHER and Acc-PANTHER algorithms, along with their advantages in facilitating PNT services within the operational contexts of search and rescue and military operations. Specifically, Section VI-A presents the fundamental operation and performance characteristics of the A-PANTHER and Acc-PANTHER algorithms across various target formations in the operational field. Section VI-B addresses the scalability aspect, and Section VI-C offers a comparative evaluation of the Acc-PANTHER algorithm in relation to alternative PNT

solutions. We analyze different formations for a squad of 15 members departing from an FOB, where initially they are organized in a "file" formation, and they proceed on a reconnaissance mission, organized in "line", "echelon", "column", and "wedge" formations under different patrolling circumstances. In all these formations, three fireteams are established, each consisting of 5 members, with a 5 m separation between fireteam members and a 10 m gap between fireteams. The following simulation parameters have been used: $S = 10$, radius of FOB: 75 [m], $N = 15$, $N_{\max} = 3$ $\forall k \in \mathcal{K}$, $W = 0.25$ [GHz], $f_c = 24.125$ [GHz] $B = 1500$ [bits], $P_s = 10$ [W], $N_0 = -175$ $[\frac{dBm}{Hz}]$ with $I_0 = W \cdot N_0 = 7.91 \cdot 10^{-13}$ [W], $\lambda = 0.5$, $w_1 = 0.9$, $w_2 = 0.1$, and the channel gain $G_{s,n}$ follows the 3GPP standard considering the worst case scenario of an urban micro street canyon environment [36], unless otherwise explicitly stated. The choice of 1500 bits as the signal size reflects the minimal data required for the PNT services, as the targets primarily receive pilot/beacon signals with only essential information, i.e., anchor ID and anchor node's position coordinates. Also, a Monte Carlo analysis of 1,000 executions of the overall model has been performed to derive all the presented results.

A. PURE OPERATION OF PANTHER FRAMEWORK

Fig. 2(a)-2(d), Fig. 3(a)-3(d), and Fig. 4(a)-4(d) show the targets' accurate utility (Eq. (2)), the anchor nodes' accurate utility (computed using Eq. (3)), and the total delay of each target (Eq. (1)), respectively, as *initially* derived from the outcome of the A-PANTHER algorithm, while the targets were residing within the FOB in the file formation (the normalization in Eq. (2) was performed with respect to the real targets' formations in the field), and the final achieved values after the power optimization, when the targets are organized in line, echelon, column, and wedge formation in the operational field, respectively. In Fig. 2(a)-2(d), a higher target accurate utility is ideally desirable for all the targets and the overall trend observed reveals that the targets in close proximity to the anchor nodes, achieve higher target accurate utilities. Also, in Fig. 3(a)-3(d), a higher accurate utility is desirable for all the anchor nodes which have been selected by the plethora of targets. And, in Fig. 4(a)-4(d), a lower total delay for reception of the beacon signals is ideally desirable among all the targets and their associated anchor nodes. Also, it is noted that the shape/distribution of the target accurate utilities, anchor nodes' accurate utilities, and the total delays in Fig. 2(a)-4(d) characterize a corresponding formation. In fact, the results show that targets in closer proximity to the FOB experience increased accurate utility when employing the Acc-PANTHER algorithm compared to the outcomes derived from the A-PANTHER approach (Fig. 2(e)). Furthermore, the results illustrate that the proposed Acc-PANTHER algorithm combined with the Acc-PANTHER Power algorithm results in only a marginal reduction in the accurate utility for the targets undertaking patrols in the field, even for those located at significant distances from the anchor nodes (i.e., large ID targets across all formations). Also, the results show that the anchor nodes' accurate utility improves through the switching operations and the power optimization (Fig. 3(e)). Moreover, the anchor nodes serving a larger number of targets experience an increase in their experienced utility, as the first term in Eq. (3) is increased with a higher target count. Thus, the overall effect is an increase in the anchor nodes' utility when serving a greater number of targets. Moreover, it is observed that through the power optimization, each anchor node on average lowers the power level because of the associated cost of transmitting at higher power levels (the second term in Eq. (3)). Since most of the anchor nodes transmit with lower power, there is a reduction in the mutual interference which improves the transmission delay for each target (Fig. 4(e)).

Fig. 5(a)-5(d) depict the constellation average utility (Definition 3), total execution time for A-PANTHER, Acc-PANTHER and Acc-PANTHER Power algorithms, average

$$
\begin{aligned}
\frac{\partial^2 U_s}{\partial {P_{s'}}^2} = \sum_{\forall n \in N_s} \Bigg(& \frac{\alpha\gamma}{\left(\gamma \sum_{\boldsymbol{\sigma}_n} t_{s,n} + \beta\right)^3} \frac{\gamma B \ln 2 G_{s',n} P_s G_{s,n}}{W \ln^2\left(1 + \frac{P_s G_{s,n}}{\sum_{s' \neq s} P_{s'} G_{s',n} + I_0}\right)\left(\sum_{s' \neq s} P_{s'} G_{s',n} + I_0 + P_s G_{s,n}\right)\left(\sum_{s' \neq s} P_{s'} G_{s',n} + I_0\right)} \\
& \frac{B \ln 2 G_{s',n} P_s G_{s,n}}{W \ln^2\left(1 + \frac{P_s G_{s,n}}{\sum_{s' \neq s} P_{s'} G_{s',n} + I_0}\right)\left(\sum_{s' \neq s} P_{s'} G_{s',n} + I_0 + P_s G_{s,n}\right)\left(\sum_{s' \neq s} P_{s'} G_{s',n} + I_0\right)} \\
& + \frac{\alpha\gamma}{\left(\gamma \sum_{\boldsymbol{\sigma}_n} t_{s,n} + \beta\right)^2} \frac{B \ln 2 G_{s',n} P_s G_{s,n}}{W \left[\ln^2\left(1 + \frac{P_s G_{s,n}}{\sum_{s' \neq s} P_{s'} G_{s',n} + I_0}\right)\left(\sum_{s' \neq s} P_{s'} G_{s',n} + I_0 + P_s G_{s,n}\right)\left(\sum_{s' \neq s} P_{s'} G_{s',n} + I_0\right)\right]^2} \\
& G_{s',n} \ln\left(1 + \frac{P_s G_{s,n}}{\sum_{s' \neq s} P_{s'} G_{s',n} + I_0}\right) \Bigg[-2 P_s G_{s,n} + \ln\left(1 + \frac{P_s G_{s,n}}{\sum_{s' \neq s} P_{s'} G_{s',n} + I_0}\right)\left(\sum_{s' \neq s} P_{s'} G_{s',n} + I_0\right) \\
& + \ln\left(1 + \frac{P_s G_{s,n}}{\sum_{s' \neq s} P_{s'} G_{s',n} + I_0}\right)\left(\sum_{s' \neq s} P_{s'} G_{s',n} + I_0 + P_s G_{s,n}\right) \Bigg] \Bigg) > 0
\end{aligned} \tag{10}
$$

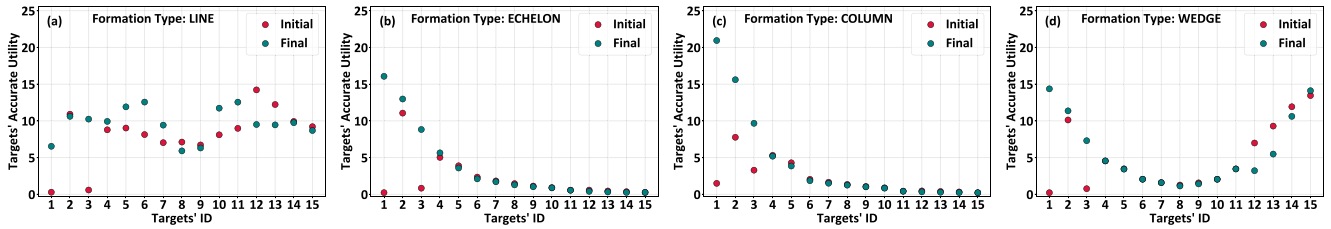

FIGURE 2. Targets' accurate utility (Eq. (2)) under different targets' formations in the operational field.

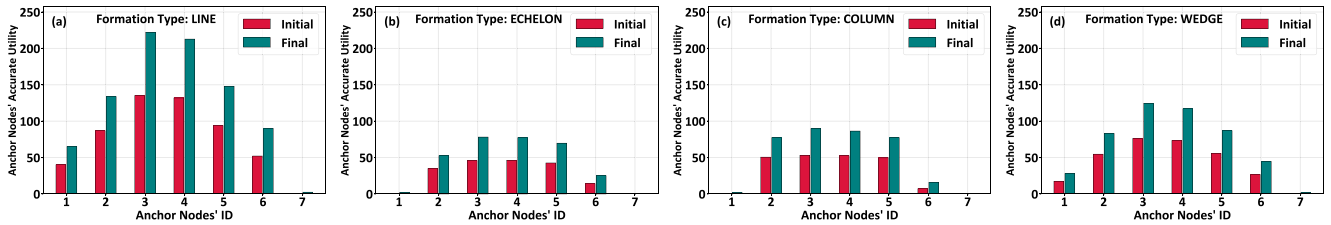

FIGURE 3. Anchor nodes' accurate utility (Eq. (3)) under different targets' formations in the operational field.

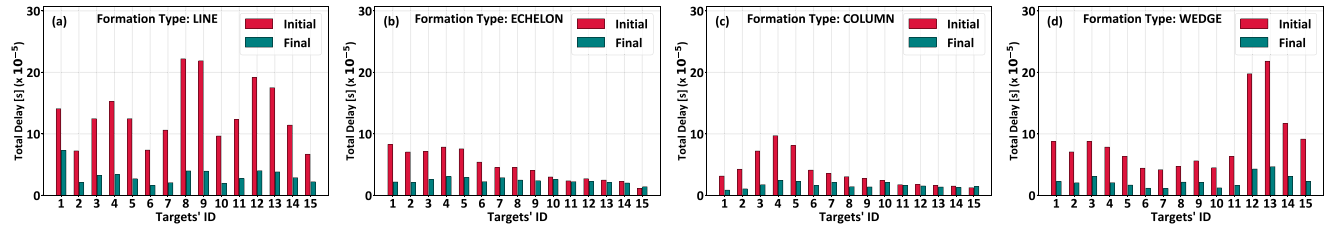

FIGURE 4. Targets' total delay (Eq. (1)) under different targets' formations in the operational field.

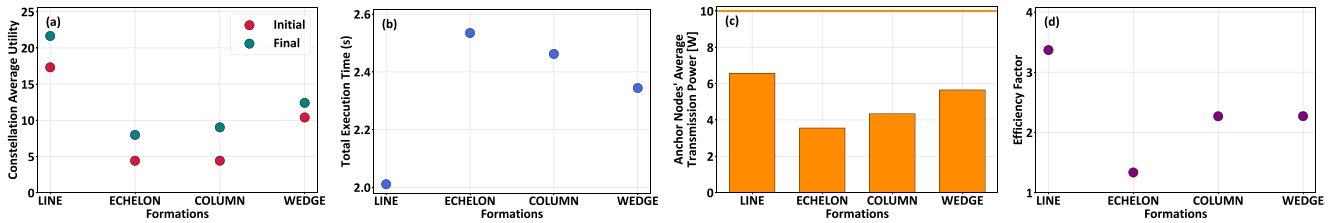

FIGURE 5. Average constellation utility, total execution time, average transmission power of the anchor nodes, and efficiency factor under different targets' formations in the operational field.

transmission power of the anchor nodes, and the efficiency factor (Eq. (11)) under the four examined formations in the operational field, respectively. The efficiency factor is defined as follows:

$$\eta = \frac{\frac{\sum_{\forall c \in \mathcal{C}} \mathcal{U}(c)}{|\mathcal{C}|}}{T \cdot \left(\frac{\sum_{\forall n \in \mathcal{N}} \sum_{\sigma_n} t_{s,n}}{N} \right)} \tag{11}$$

where, T is the total execution time.

The results demonstrate that the constellation utility improves on average for each formation considering also the power optimization, compared to the average utility when the targets were arranged in a "file" formation within the FOB (Fig. 5). It is highlighted that the "line" formation achieves the highest constellation average utility and the lowest total execution time. This observation stems from the uniform distribution of the targets across the operational field under the "line" formation which enables a near-uniform association of the targets with the anchor nodes. In this case, the distances between each target and its assigned anchor node are almost equal which results in higher constellation's average utility. Additionally, the "line" formation is characterized by the shortest total execution time, as the primary factor influencing the execution time is the duration required for the power algorithm (Algorithm 3), which is minimized in this formation. Specifically, as shown in Fig. 5(c), the transmission power of the anchor nodes, on average, is higher when the targets are organized in the "line" formation. This is because the anchor nodes, serving a similar number of targets, converge more rapidly to similar transmission power levels. In contrast, in the "echelon" formation, higher-ID targets are farther from the anchor nodes, and they require more time to converge to their power levels. In summary, the "line" formation is the

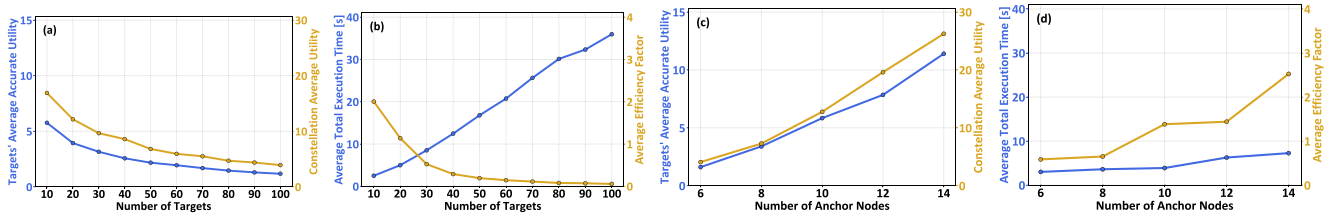

FIGURE 6. Scalability Analysis.

most efficient for patrolling and providing PNT services, as it results in the highest constellation utility, the shortest execution time, and the lowest average total delay.

B. SCALABILITY ANALYSIS

In this section, a scalability analysis is performed to demonstrate the adaptability of the PANTHER framework in cases of large-scale operations in the field, both in terms of a large number of targets and anchor nodes. Fig. 6(a)-6(d) depict the targets' accurate utilities, constellation utilities, total execution time, and efficiency factor of the PANTHER framework averaged over all the formations to observe the general trends for an increasing number of targets (considering 10 anchor nodes) and an increasing number of anchor nodes (considering 15 targets), respectively.

Fig. 6(a)-6(b) show that as the number of targets increases, the targets' average accurate utilities decreases as the mutual interference increases which increases the overall transmission delay for each target. Since, the constellation utility depends on the total accurate utilities of the targets served by the constellation, the constellation utility correspondingly decreases as the number of targets increases. In this case, when the total number of targets in the system are increasing, the number of anchor nodes remain constant. So, for increasing number of targets, the same number of anchor nodes have to serve the increased number of targets which increases the time required for the power algorithm (Algorithm 3) to converge and so, the average total execution time of the system increases with the increasing number of targets. Also, since the average constellation utility decreases, and simultaneously, the average total execution time and average transmission delay increases, the average efficiency factor (Eq. (11)) of the overall system decreases with the increasing number of targets.

Fig. 6(c)-6(d) reveal that as the number of anchor nodes in the system increases (keeping the same number of targets), the targets' average accurate utilities increase as the targets can exploit the higher diversity among the anchor nodes. In other words, with the increasing number of anchor nodes, the targets have more suitable options (anchor nodes in closer proximity) to choose from and also, the instances, where the constellation chosen by a target has already reached its limit ($N_{\max}$), decrease. This means that each target can be assigned a more suitable constellation in terms of proximity which increases the targets' average accurate utilities and also the average constellation utilities. Furthermore, with the increasing number of anchor nodes, the number of targets served by each anchor node reduces which enables the anchor node to find a power more quickly leading to a relatively slower increment in the average total execution time for an increasing number of anchor nodes. Finally, due to the increasing average constellation utility and relatively slower increments in the average total execution time, the efficiency factor of the overall system increases. This analysis provides us a valuable insight that as the number of targets in the system increases, the number of anchor nodes should also be ideally increased to maintain a balanced value of the efficiency factor for all the four examined formations in the operational field.

C. COMPARATIVE SCENARIOS

In this section a comparative evaluation of the PANTHER framework is performed against three comparative scenarios: (i) ACC-PANTHER: the targets select constellations following the Acc-PANTHER algorithm but does not execute the Acc-PANTHER Power algorithm, (ii) MIN LATENCY: the targets select constellations following the Acc-PANTHER algorithm, where their accurate utility is captured as the inverse of the overall delay to receive the beacon signals from the anchor nodes; and (iii) RANDOM: the targets randomly select constellations. Fig. 7(a)-7(d) present the constellation average utility, total execution time, average total delay, and efficiency factor for all the four examined formations in the operational field.

Fig. 7 reveals that the average constellation utility achieved is the highest for the PANTHER framework which proves that the target accurate utilities improve most with the PANTHER framework compared to other scenarios. However, Fig. 7(b) shows that the total execution time of PANTHER framework is higher than the ACC-PANTHER scenario since in this scenario, the Acc-PANTHER Power algorithm is not executed which dominates the total execution time and thus, resulting in the lowest total execution time for the ACC-PANTHER scenario. Furthermore, it is observed from Fig. 7(c) that the lowest average total delay is achieved through the PANTHER framework since this framework is jointly benefited by the Acc-PANTHER switching operations (Algorithm 2) and the Acc-PANTHER Power algorithm (Algorithm 3) leading to constellation selections by the targets as well as transmission powers chosen by the anchor nodes. Although the ACC-PANTHER scenario is benefited by the Acc-PANTHER algorithm (Algorithm 2), it fails to

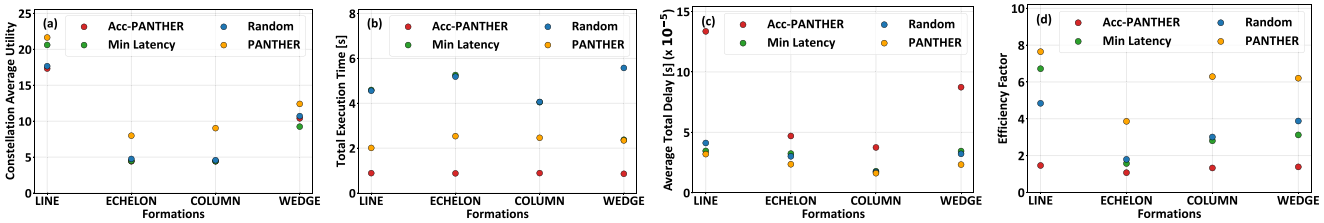

FIGURE 7. Comparative Evaluation.

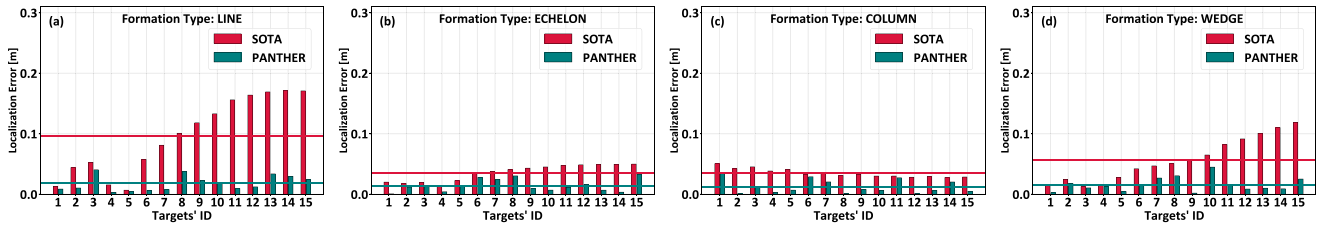

FIGURE 8. Comparative Evaluation to the Iterative Least Squares Algorithm.

reduce the mutual interference and so, the average total delay is highest. As all the other scenarios except scenario (i) (ACC-PANTHER) utilizes the Acc-PANTHER Power algorithm, they experience relatively lower average total delay which further signifies the importance of the Acc-PANTHER Power algorithm. Finally, Fig. 7(d) reveals that the highest efficiency factor for all the four examined formation is achieved under the PANTHER framework which proves that the PANTHER framework is the most ideal framework for providing fast and reliable PNT services to the targets in patrol.

To evaluate the performance of the proposed PANTHER approach in target localization, we compared it against a state-of-the-art method referred to as SOTA, which has been used in several existing research works, e.g., [42], [43], [44]. In the SOTA method, the targets utilize the beacon signals received from all the nearby anchor nodes to calculate their pseudoranges, which are then processed using the Iterative Least Squares (ILS) algorithm to estimate their positions. The ILS algorithm is widely recognized for its effectiveness in localization tasks involving unknown coordinates [41].

Fig. 8(a)-8(d) illustrate the localization error, defined as the absolute difference between the actual and predicted target positions (including the clock offsets), for both the PANTHER and SOTA approaches across various patrol formations. Additionally, the horizontal lines in the figures indicate the average localization error for each method. In this simulation, the targets' initial estimated positions were assumed to be their locations at the Forward Operating Base (FOB), corresponding to the file formation. The added noise in the beacon signals was modeled as a function of the SINR. Higher SINR values corresponded to lower noise levels, reflecting the impact of anchor transmission power and channel gain conditions.

For all the targets and formations, the localization error observed with the PANTHER approach was consistently lower than that of the SOTA method. This improvement is primarily attributed to the PANTHER algorithm's ability to select a limited subset of anchor nodes based on factors such as relative distances, channel gains, and total delays between anchors and targets. This selection process is driven by advanced matching algorithms (A-PANTHER and Acc-PANTHER). Furthermore, the Acc-PANTHER Power Control mechanism optimizes anchor transmission power, reducing the total delays, as demonstrated in Fig. 4(a)-4(d). By improving the signal reception and minimizing the delays, the PANTHER approach achieves a significant reduction in localization error and provides superior accuracy for the targets' positioning.

VII. CONCLUSION AND FUTURE WORK

In conclusion, in this paper, the PANTHER framework is introduced to effectively address the challenges of GPS-denied environments by integrating matching theory, coalition game models, and power optimization techniques to deliver a robust Position, Navigation, and Timing solution. Through the introduction of the A-PANTHER and Acc-PANTHER frameworks, our research presents innovative methods for both initial and extended operations, enabling the precise target positioning and anchor nodes' selection in dynamic scenarios. The system's power optimization further enhances the anchor nodes' performance and ensures the efficient resource utilization while minimizing positioning errors. Comprehensive performance evaluations, including simulations, are presented and confirm the scalability and practical applicability of the PANTHER framework across diverse target formations. Our experiments demonstrate the PANTHER's potential for critical search-and-rescue and military operations in complex environments. Part of our current and future work is the deployment of the PANTHER framework in a featureless terrain with ad-hoc developed anchor nodes and mobile targets to test

PANTHER's robustness under diverse mobility scenarios. Also, we will explore adaptive anti-jamming strategies and frequency-hopping techniques to enhance the PANTHER's resilience against signal interference in warfare environments where the link quality can be compromised by intentional jamming.

REFERENCES

[1] S. E. Trevlakis et al., "Localization as a key enabler of 6g wireless systems: A comprehensive survey and an outlook," *IEEE Open J. Commun. Soc.*, vol. 4, pp. 2733–2801, 2023.

[2] T. Ma, Y. Xiao, X. Lei, L. Zhang, Y. Niu, and G. K. Karagiannidis, "Reconfigurable intelligent surface-assisted localization: Technologies, challenges, and the road ahead," *IEEE Open J. Commun. Soc.*, vol. 4, pp. 1430–1451, 2023.

[3] V. P. Rekkas et al., "Artificial intelligence in visible light positioning for indoor IoT: A methodological review," *IEEE Open J. Commun. Soc.*, vol. 4, pp. 2838–2869, 2023.

[4] R. C. Shit, S. Sharma, K. Yelamarthi, and D. Puthal, "AI-enabled fingerprinting and crowdsource-based vehicle localization for resilient and safe transportation systems," *IEEE Trans. Intell. Transp. Syst.*, vol. 22, no. 7, pp. 4660–4669, Jul. 2021.

[5] A. Blaga, F. Campolo, M. Rea, and X. Costa-Pérez, "3DSAR+: A single-drone 3D cellular search and rescue solution leveraging 5G-nr," *IEEE Open J. Commun. Soc.*, vol. 5, pp. 4808–4822, 2024.

[6] I. D. Miller, F. Cladera, T. Smith, C. J. Taylor, and V. Kumar, "Air-ground collaboration with SPOMP: Semantic panoramic online mapping and planning," *IEEE Trans. Field Robot.*, vol. 1, pp. 93–112, 2024.

[7] B. Sun, B. Tan, M. Ashraf, M. Valkama, and E. S. Lohan, "Embedding the localization and imaging functions in mobile systems: An airport surveillance use case," *IEEE Open J. Commun. Soc.*, vol. 3, pp. 1656–1671, 2022.

[8] R. Jia, K. Xu, X. Xia, W. Xie, N. Sha, and W. Guo, "Extrinsic information aided fingerprint localization of vehicles for cell-free massive MIMO-OFDM system," *IEEE Open J. Commun. Soc.*, vol. 3, pp. 1810–1819, 2022.

[9] W. Zhang and W. Zhang, "An efficient UAV localization technique based on particle swarm optimization," *IEEE Trans. Veh. Technol.*, vol. 71, no. 9, pp. 9544–9557, Sep. 2022.

[10] Y. Chen and J. Jiang, "An oblique-robust absolute visual localization method for GPS-denied UAV with satellite imagery," *IEEE Trans. Geosci. Remote Sens.*, vol. 62, 2024, Art. no. 5601713, doi: 10.1109/TGRS.2023.3342142.

[11] X. Wan, Y. Shao, S. Zhang, and S. Li, "Terrain aided planetary UAV localization based on geo-referencing," *IEEE Trans. Geosci. Remote Sens.*, vol. 60, Aug. 2022, Art. no. 4602018.

[12] T. Wang, L.-H. Shi, S. Qiu, Z. Sun, Q. Zhang, and Y. Li, "Time delay correction for the MARCOS lightning VHF mapping array system," *IEEE Trans. Electromagn. Compat.*, vol. 63, no. 6, pp. 1981–1988, Dec. 2021.

[13] H. Zhang, S. Mao, D. Niyato, and Z. Han, "Location-dependent augmented reality services in wireless edge-enabled metaverse systems," *IEEE Open J. Commun. Soc.*, vol. 4, pp. 171–183, 2023.

[14] A. Jehangir, S. M. Majid Ashraf, R. A. Khalil, and N. Saeed, "ISAC-enabled underwater IoT network localization: Overcoming asynchrony, mobility, and stratification issues," *IEEE Open J. Commun. Soc.*, vol. 5, pp. 3277–3288, 2024.

[15] B. Cenikliogl u, D. A. Tubail, A. E. Canbilen, I. Develi, and S. S. Ikki, "Error analysis of the joint localization and synchronization of RIS-assisted mm-Wave MISO-OFDM under the effect of hardware impairments," *IEEE Open J. Commun. Soc.*, vol. 3, pp. 2151–2161, 2022.

[16] G. Mylonopoulos, L. Venturino, S. Buzzi, and C. D'Andrea, "Estimation of the user position and orientation in mmwave cellular networks aided by an active RIS," *IEEE Open J. Commun. Soc.*, vol. 5, pp. 4868–4884, 2024.

[17] Y.-E. Chen, H.-H. Liew, J.-C. Chao, and R.-B. Wu, "Decimeter-accuracy positioning for drones using two-stage trilateration in a GPS-denied environment," *IEEE Internet Things J.*, vol. 10, no. 9, pp. 8319–8326, May 2023.

[18] D. A. Tubail, M. El-Absi, S. Ikki, and T. Kaiser, "Hardware-aware joint localization-synchronization and tracking using reconfigurable intelligent surfaces in 5G and beyond," *IEEE Open J. Commun. Soc.*, vol. 5, pp. 1899–1915, 2024.

[19] K. Li, M. El-Hajjar, and L.-L. Yang, "Reconfigurable intelligent surface aided position and orientation estimation based on joint beamforming with limited feedback," *IEEE Open J. Commun. Soc.*, vol. 4, pp. 748–767, 2023.

[20] Y. Huang, M. Safari, H. Haas, and I. Tavakkolnia, "Optical wireless 3-D-positioning and device orientation estimation," *IEEE Open J. Commun. Soc.*, vol. 5, pp. 4519–4530, 2024.

[21] A. Fadakar, M. Sabbaghian, and H. Wymeersch, "Multi-RIS-assisted 3D localization and synchronization via deep learning," *IEEE Open J. Commun. Soc.*, vol. 5, pp. 3299–3314, 2024.

[22] Y. Wu, Y. Li, W. Li, H. Li, and R. Lu, "Robust lidar-based localization scheme for unmanned ground vehicle via multisensor fusion," *IEEE Trans. Neural Netw. Learn. Syst.*, vol. 32, no. 12, pp. 5633–5643, Dec. 2021.

[23] J. Cheng, C. Wang, and M. Q.-H. Meng, "Robust visual localization in dynamic environments based on sparse motion removal," *IEEE Trans. Autom. Sci. Eng.*, vol. 17, no. 2, pp. 658–669, Apr. 2020.

[24] R. A. Khalil and N. Saeed, "Robust multi-target localization in ISAC systems: Leveraging multidimensional scaling," *IEEE Open J. Commun. Soc.*, vol. 5, pp. 3678–3689, 2024.

[25] H. Hosseinianfar and M. Brandt-Pearce, "Cooperative passive pedestrian detection and localization using a visible light communication access network," *IEEE Open J. Commun. Soc.*, vol. 1, pp. 1325–1335, 2020.

[26] K. Li, M. El-Hajjar, and L.-l. Yang, "Millimeter-wave based localization using a two-stage channel estimation relying on few-bit adcs," *IEEE Open J. Commun. Soc.*, vol. 2, pp. 1736–1752, 2021.

[27] Q. Wu, Y. Wan, Z. Zheng, Y. Zhang, G. Wang, and Z. Zhao, "Camp: A cross-view geo-localization method using contrastive attributes mining and position-aware partitioning," *IEEE Trans. Geosci. Remote Sens.*, vol. 62, Aug. 2024, Art. no. 5637614.

[28] S. Zhang, R. Cui, W. Yan, and Y. Li, "Dual-layer path planning with pose slam for autonomous exploration in gps-denied environments," *IEEE Trans. Ind. Electron.*, vol. 71, no. 5, pp. 4976–4986, May 2024.

[29] L. Ruan et al., "Cooperative relative localization for UAV swarm in GNSS-denied environment: A coalition formation game approach," *IEEE Internet Things J.*, vol. 9, no. 13, pp. 11560–11577, Jul. 2022.

[30] H. Shen, Q. Zong, B. Tian, and H. Lu, "Voxel-based localization and mapping for multirobot system in GPS-denied environments," *IEEE Trans. Ind. Electron.*, vol. 69, no. 10, pp. 10333–10342, Oct. 2022.

[31] *The Ranger Handbook: TC 3-21.76*, United States Dept. Army, Fort Benning, GA, USA, 2017.

[32] M. S. Hossain, N. Irtija, E. E. Tsiropoulou, J. Plusquellic, and S. Papavassiliou, "Reconfigurable intelligent surfaces enabling positioning, navigation, and timing services," in *Proc. IEEE Int. Conf. Commun. (ICC)*, 2022, pp. 4625–4630.

[33] J. B. Rosen, "Existence and uniqueness of equilibrium points for concave n-person games," *Econometrica, J. Econometr. Soc.*, vol. 33, no. 3, pp. 520–534, 1965.

[34] J. C. Goodman, "A note on existence and uniqueness of equilibrium points for concave *N*-person games," *Econometrica*, vol. 48, no. 1, p. 251, 1980.

[35] E. E. Tsiropoulou, G. K. Katsinis, and S. Papavassiliou, "Utility-based power control via convex pricing for the uplink in CDMA wireless networks," in *Proc. Eur. Wireless Conf.*, 2010, pp. 200–206.

[36] "5G; study on channel model for frequencies from 0.5 to 100 GHz; (Release 16), Version 16.1.0," 3GPP, Sophia Antipolis, France, Rep. TR 38.901, 2020.

[37] B. Yang, E. Yang, H. Shi, L. Yu, and C. Niu, "Adaptive square-root cubature Kalman filter based low cost UAV positioning in dark and GPS-denied environments," *IEEE Trans. Intell. Veh.*, early access, Sep. 10, 2024, doi: 10.1109/TIV.2024.3457678.

[38] M. Irfan, S. Dalai, P. Trslic, M. C. Santos, J. Riordan, and G. Dooly, "LGVINS: LiDAR-GPS-visual and inertial system based multi-sensor fusion for smooth and reliable UAV state estimation," *IEEE Trans. Intell. Veh.*, early access, Sep. 27, 2024, doi: 10.1109/TIV.2024.3469551.

[39] Y. Wang, Q. Yang, H. Cui, and H. Fang, "Relative localization with non-persistent excitation using UWB-IMU measurements," *IEEE Trans. Autom. Sci. Eng.*, early access, Sep. 25, 2024, doi: 10.1109/TASE.2024.3460811.
[40] A. Famili, A. Stavrou, H. Wang, and J.-M. Park, "PILOT: High-precision indoor localization for autonomous drones," *IEEE Trans. Veh. Technol.*, vol. 72, no. 5, pp. 6445–6459, May 2023.
[41] B. Pardhasaradhi, P. Srihari, and P. Aparna, "Navigation in GPS spoofed environment using M-best positioning algorithm and data association," *IEEE Access*, vol. 9, pp. 51536–51549, 2021.
[42] M. Cui et al., "A novel iterative positioning method based on difference RSS model with 5G field experiments," *IEEE Sensors J.*, vol. 24, no. 5, pp. 5466–5475, Mar. 2024.
[43] J. Wang et al., "SLAM-based joint calibration of multiple asynchronous microphone arrays and sound source localization," *IEEE Trans. Robot.*, vol. 40, pp. 4024–4044, 2024, doi: 10.1109/TRO.2024.3410456.
[44] J. Yan, X. Tian, X. Luo, and X. Guan, "Design of an embedded communication system for underwater asynchronous localization," *IEEE Embed. Syst. Lett.*, vol. 11, no. 3, pp. 97–100, Sep. 2019.

MD SADMAN SIRAJ (Graduate Student Member, IEEE) received the bachelor's degree in electrical and electronic engineering from the University of Dhaka, Dhaka, Bangladesh, in 2020, and the master's degree in computer engineering from the University of New Mexico, Albuquerque, NM, USA, in 2021. He is currently pursuing the Ph.D. degree with the School of Electrical, Computer and Energy Engineering, Arizona State University, where he is also a Research Assistant. His research interests include alternative positioning, navigation, and timing services, resource management in wireless networks, game theory, and reinforcement learning.

JOSHUA R. ATENCIO (Graduate Student Member, IEEE) received the bachelor's degree in electrical engineering and the master's degree in electrical engineering from the University of New Mexico, Albuquerque, NM, USA, in 2020 and 2022, respectively, where he is currently pursuing the Ph.D. degree in computer engineering. He is a Staff Computer Scientist with Sandia National Laboratories, where he conducts research in applying machine learning to automatic target recognition systems. His broader research interests are in the intersection of positioning, navigation, and timing and autonomous systems.

EIRINI ELENI TSIROPOULOU (Senior Member, IEEE) is currently an Associate Professor with the School of Electrical, Computer and Energy Engineering, Arizona State University. Her main research interests lie in the area of cyber–physical social systems and wireless heterogeneous networks, with an emphasis on network modeling and optimization, resource orchestration in interdependent systems, reinforcement learning, game theory, network economics, and Internet of Things. Four of her papers received the Best Paper Award at IEEE WCNC in 2012, ADHOCNETS in 2015, IEEE/IFIP WMNC 2019, and INFOCOM 2019 by the IEEE ComSoc Technical Committee on Communications Systems Integration and Modeling. She received the NSF CRII Award in 2019 and the Early Career Award by the IEEE Communications Society Internet Technical Committee in 2019. In 2017, she was selected by the IEEE Communication Society—N2Women—as one of the Top Ten Rising Stars in the communications and networking field.